Special Collection

Ionic Diode and Molecular Pump Phenomena Associated with Caffeic Acid Accumulated into an Intrinsically Microporous Polyamine (PIM-EA-TB)

Zhongkai Li,[a] Lina Wang,[a] Richard Malpass-Evans,[b] Mariolino Carta,[c] Neil B. McKeown,[b] Klaus Mathwig,[d] Philip J. Fletcher,[e] and Frank Marken*[a]

The polymer of intrinsic microporosity PIM-EA-TB provides a molecularly rigid micropore structure containing tertiary amine sites and is shown here to interact with hydrogen bonding guest molecules such as caffeic acid. Voltammetric data with a PIM-EA-TB film on glassy carbon electrodes show that in both acidic solution (pH 2; PIM-EA-TB is protonated) and in neutral solution (pH 6; PIM-EA-TB is not protonated) caffeic acid is slowly accumulated into the microporous host. Binding constants are estimated and suggested to be linked to hydrogen bonding causing accumulation of caffeic acid. When employing PIM-EA-TB as an asymmetric membrane coated onto a 5 μm thick Teflon support film with 10 μm diameter microholes (using either a single microhole or a 10×10 array of microholes), binding of caffeic acid is shown to cause a modulation of the ionic current without affecting the pH-dependent ionic diode behaviour. Two complementary types of effects of caffeic acid guests are discussed based on blocking anion diffusion pathways and based on removal of positive charges. The caffeic acid transport mechanism/efficiency is investigated in view of selective molecular pumping.

1. Introduction

Ionic diode or rectifier effects are observed in nanocone[1] and nanopore[2] devices as well as in microscale or macroscale systems based on porous materials with semi-permeability, asymmetry, and a potential dependent resistivity.[3] Steady state diffusion phenomena in microhole devices provide experimental conditions for ionic diode devices to be studied with different types of ionomer materials such as Nafion,[4] graphene oxide,[5] cellulose,[6] carbon nanofibers,[7] or bio-aggregates based on bacteriophages.[8] The experimental four-electrode measurement cell for microhole processes is illustrated in Figure 1A with an ionomer material attached asymmetrically to a Teflon film with a laser-drilled microhole. Here, employing this approach, binding and transport of guest molecules in the polymer of intrinsic microporosity PIM-EA-TB are investigated.[9]

Polymers of intrinsic microporosity (PIMs) provide a recently developed class of synthetic membrane materials with high internal surface area and rigid micropore structure for applications in gas separation[10] and in electrochemistry.[11] The highly rigid polymer backbone provides open porosity comparable to that in zeolitic structures combined with the ability to form films and coatings simply by solution casting. PIM-EA-TB (see molecular structure in Figure 1) derives from an ethano-

[a] Z. Li, L. Wang, Prof. F. Marken
Department of Chemistry
University of Bath
Claverton Down, Bath BA2 7AY, UK
E-mail: f.marken@bath.ac.uk
[b] R. Malpass-Evans, Prof. N. B. McKeown
EaStCHEM, School of Chemistry
University of Edinburgh, Joseph Black Building
David Brewster Road, Edinburgh, Scotland EH9 3JF, UK
[c] Dr. M. Carta
Department of Chemistry
Swansea University, College of Science, Grove Building
Singleton Park, Swansea SA2 8PP, UK
[d] Dr. K. Mathwig
Stichting imec Nederland within OnePlanet Research Center
Bronland 10, 6708 WH Wageningen, The Netherlands
[e] Dr. P. J. Fletcher
University of Bath
Materials & Chemical Characterisation Facility MC2
Bath BA2 7AY, UK

Special Collection
An invited contribution to the Marcin Opałło Festschrift

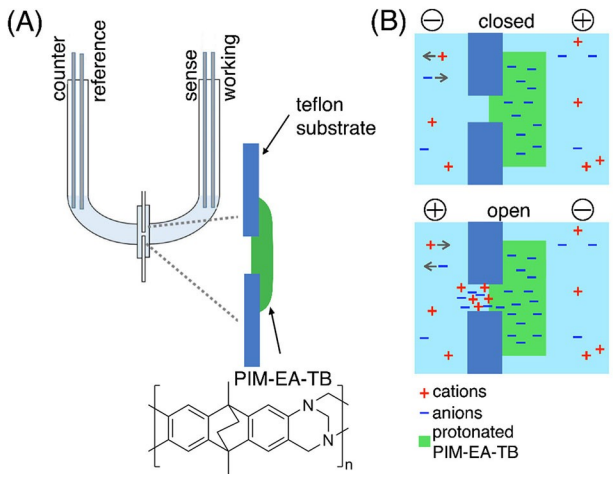

Figure 1. (A) Schematic drawing of a four-electrode measurement cell with asymmetrically applied PIM-EA-TB on a microhole in Teflon. (B) Illustration of the "closed" and "open" states of the diode for the case of a positively charged semipermeable membrane material such as protonated PIM-EA-TB.

anthracene (EA) structural motif formed in a Tröger base (TB) reaction[12] and offers microchannels with typically 1–2 nm diameter and a surface area of typically 1000 $m^2 g^{-1}$ (based on nitrogen adsorption isotherm data[13]). Applications for PIM-EA-TB and related materials have been proposed in redox flow cell membranes,[14] as a precursor for microporous heterocarbons,[15,16] and as protective layer on fuel cell catalysts.[17] Previous ionic diode experiments with the polymer of intrinsic microporosity PIM-EA-TB[9] have shown that in neutral solution no semi-permeability is observed. Both cations and anions can permeate and produce ion current responses. When the solution pH is lowered to 4 or below, protonation of the tertiary amine sites occurs, and PIM-EA-TB turns into an anion semi-permeable material[9] with ionic diode or ionic rectifier behaviour. The proposed mechanism for this behaviour is illustrated in Figure 1B for the case of positive applied potentials at the working electrode leading to anions moving from the counter electrode compartment which causes depletion and high resistivity in the microhole region ("closed" state). In contrast, when applying a negative potential at the working electrode, anions (and cations) are accumulated from the ionomer material (and from the adjacent solution) into the microhole region causing locally low resistivity ("open" state).[18]

In this study, the effect of hydrogen bonding guest molecules such as caffeic acid on the PIM-EA-TB ionic diode behaviour and molecular transport are investigated. It has recently been reported that guest species such as $Fe(CN)_6^{4-/3-}$ can be accumulated and bound into PIM-EA-TB pores via hydrogen bonds.[19] It is shown here that other species such as caffeic acid readily accumulate. Furthermore, the hydrogen bonding host-guest interactions modify the transport processes during ion transport. Caffeic acid here (although itself of interest in medicine)[20,21] has to be seen as a model system for other related drug or active molecular species. The accumulation of caffeic acid into the PIM-EA-TB microchannels changes anion transport rates and may lead to a voltage-driven caffeic acid pump.

Experimental Section

Chemical Reagents

PIM-EA-TB was synthesised using the previously reported method.[13] Agarose was purchased from Melford Ltd. Chloroform, potassium chloride (99.0–100.5%), H_3PO_4 (85 wt%), KOH (ACS reagent, >85%), and caffeic acid (≥98.0%) were purchased from Sigma-Aldrich. Hydrochloric acid (1 M, stabilised) was purchased from Fisher Scientific. All chemical reagents were used without further purification. Aqueous solutions were prepared using ultrapure water with resistivity not less than 18.2 MΩ cm (at 20 °C) from a Thermo Scientific water purification system.

Instrumentation

Electrochemical data were recorded on a computer-controlled potentiostat (Metrohm μAutolab II) employing a conventional three-electrode system, where a Pt wire was the counter electrode, a 3 mm diameter glassy carbon disk electrode was employed as a working electrode, and a KCl-saturated calomel electrode (SCE, Radiometer REF401) acted as the reference. Membrane voltammetry experiments were performed with a four-electrode potentiostat system (Autolab PGSTAT12). For the microhole experiment, an asymmetric four-electrode membrane cell was used in which the membrane-coated Teflon film separated two half-cells, with simple carbon rods as working and counter electrode and KCl-saturated calomel (SCE) as sense and reference electrodes (see Figure 1A). In electrochemical measurements, the working electrode was always placed on the side of PIM-EA-TB membrane. Characterisation of the membrane was performed by scanning electron microscopy (SEM) and energy dispersive x-ray emission spectroscopy (EDX) on a JEOL JSM-6301F FESEM. The detection and quantification of caffeic acid in aqueous solution was performed using a HPLC-mass spectrometry system (Agilent Technologies 6545 Q-TOF LC/MS).

Procedures

Voltammetry with a PIM-EA-TB Film Immobilised onto a Glassy Carbon Electrode

A volume of 2 μL 1 mg/mL PIM-EA-TB in chloroform was deposited onto the glassy carbon electrode. Then, the electrode was immersed into a solution containing caffeic acid in 0.1 M phosphate buffer at a given pH with caffeic acid and left overnight in a refrigerator at 4 °C to equilibrate.

Voltammetry with a PIM-EA-TB Film Immobilised onto a Teflon Substrate with Microhole

A Teflon film with laser-drilled microholes (Laser Machining Ltd, Birmingham, UK) was prepared from 5 μm thick Teflon. Figure 2 shows optical microscopy images for a single microhole with 10 μm diameter (A) and for arrays of 10×10 microholes with 10 μm diameter and 200 μm pitch (B–D).

A volume of 30 μL 2 mg/mL PIM-EA-TB in chloroform was deposited onto a laser-drilled Teflon substrate on a glass substrate (pre-coated with a thin layer of 1% wt. agarose gel to prevent the PIM-EA-TB solution from penetrating through the microhole).[22] This gave a

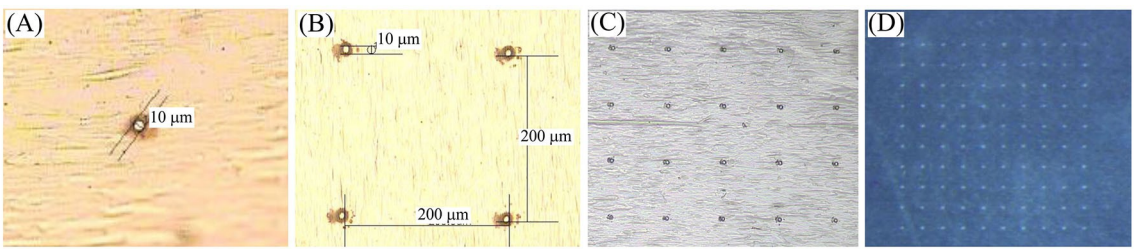

Figure 2. Optical microscopy images showing (A) a single laser-drilled microhole in Teflon and (B,C,D) a 10×10 array of microholes with a pitch of 200 μm.

uniform membrane coating over the microhole region after drying. Figure 3A shows a scanning electron micrograph (SEM) of the open or Teflon side with PIM-EA-TB underneath. Figures 3B-3D show energy dispersive elemental mapping. Fluorine is observed in the Teflon, whereas carbon and nitrogen are observed in the underlying PIM-EA-TB. The same coating methodology was applied to a 10×10 array of microholes in which 80 μL PIM-EA-TB solution was deposited to cover the array (on agarose gel). The resulting thickness of PIM-EA-TB films is estimated (assuming a density of 1 g cm^{-3}) to be typically 5 μm.

Concentration Analysis

When employing the 10×10 array of PIM-EA-TB coated microholes and with a fixed applied voltage of −1 V, the measured current was integrated with time. Samples from the counter electrode compartment solution phase were taken and the caffeic acid concentration analysed by Q-TOF LC/MS. The ratio of caffeic acid molecules transferred to ions transferred (based on current) was determined.

Computational Analysis

Finite element analysis (COMSOL Multiphysics 5.6) was employed to model a two-dimensional axisymmetric (cylindrical symmetry) 6 μm long micropore with a 10 μm diameter separating two reservoirs, and a 5 μm thick and 250 μm wide ionomer deposited asymmetrically on one side of the microhole, as reported recently.[18] Poisson-Nernst-Planck equations were solved using diffusivities 8×10^{-9} m^2 s^{-1} for H^+ cations and 2×10^{-9} m^2 s^{-1} for Cl^- anions, and a HCl concentration of 10 mM in both reservoirs.

2. Results and Discussion

2.1. Binding of Caffeic Acid into PIM-EA-TB Film Immobilised onto a Glassy Carbon Electrode

Caffeic acid is a redox active ortho-quinol which is readily oxidised to the corresponding quinone[23] (equation 1). This process is chemically reversible in aqueous solution with a redox potential with Nernstian pH-dependency.[24]

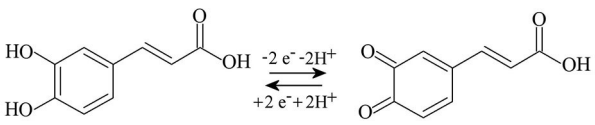

(1)

Figure 4A and 4B show cyclic voltammetry data for caffeic acid bound by adsorption into PIM-EA-TB. The immobilisation of caffeic acid is performed in 0.1 M phosphate buffer solution at pH 2 with 0.01 mM caffeic acid over 23 h at 4 °C in the dark. The voltammetric response is recorded immersed in aqueous 0.1 M phosphate buffer pH 2 at room temperature and consistent with the expected chemically reversible oxidation (see equation 1) of caffeic acid bound into the PIM-EA-TB. Voltammetric responses appear to be relatively stable with only very slow decay in peak current with time. When changing the scan rate, an approximately linear correlation of peak current with scan rate is observed (Figure 4C) indicative of an immobilised redox system with thin film behaviour (no diffusion or electron hopping effects). When integrating the charge under the voltammetric signal, $Q_p = 5.2$ μC, the number of redox active caffeic acid molecules can be estimated as 54 pmol (over a 3 mm diameter glassy carbon electrode). Assuming a 1:1 caffeic acid to polymer monomer binding interaction, this suggests a 54 pmol equivalent amount of PIM-EA-TB monomer (m.w. 274 g mol^{-1}; approximate density 1 g cm^{-3}) or a weight of 15 ng. Therefore, the thickness of the redox active film on the 3 mm diameter glassy carbon disk is only approximately 2 nm (the total average PIM-EA-TB film thickness is approximately 0.2 to 0.3 μm). Therefore, only material within tunnel distance or very close to the glassy carbon electrode surface is redox active. Charge propagation into the polymer film either by electron hopping or by molecular transport seems ineffective in this case (possibly linked to the molecularly rigid polymer backbone slowing down transport).

It is interesting to vary the caffeic acid concentration during the immobilisation process. Figure 4D shows that a concentration of 0.001 mM caffeic acid is too low, but 0.01 mM caffeic acid produced films with well-defined redox current signals. Perhaps surprisingly, a further increase in caffeic acid concentration causes lower currents and broader current peaks. These observations are consistent with an estimated Langmuirian binding constant of approximately 10^4 to10^5 mol^{-1} dm^3 (which is in a typical range for hydrogen bonding and below that for example for host-guest inclusion complexes for cyclodextrins[25]). A possible "over-crowding" effect when the micropores are saturated with caffeic acid could explain the effects observed for caffeic acid concentrations higher than 0.01 mM. This overcrowding may lower ion conductivity or electrolyte concentration in the film and thereby broaden voltammetric peaks. Data in Figure 4E demonstrate that the uptake of caffeic acid can be gradual (slowly progressing over extended periods of time) even for higher caffeic acid concentrations such as 0.1 mM. Data in Figure 4F demonstrate that the caffeic acid

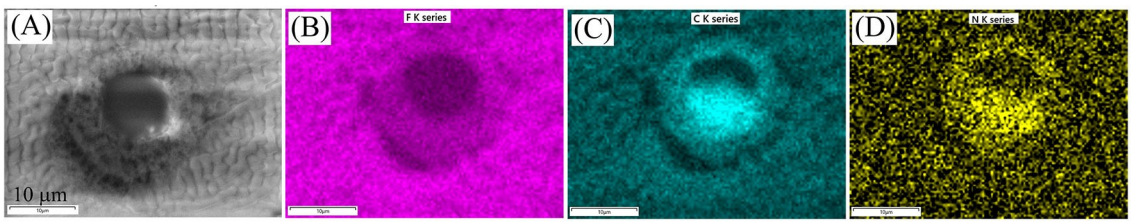

Figure 3. (A) Scanning electron microscopy (SEM) image with energy dispersive x-ray emission (EDX) mapping of elements for (B) fluorine in Teflon, (C) carbon primarily in PIM-EA-TB, and (D) nitrogen in PIM-EA-TB.

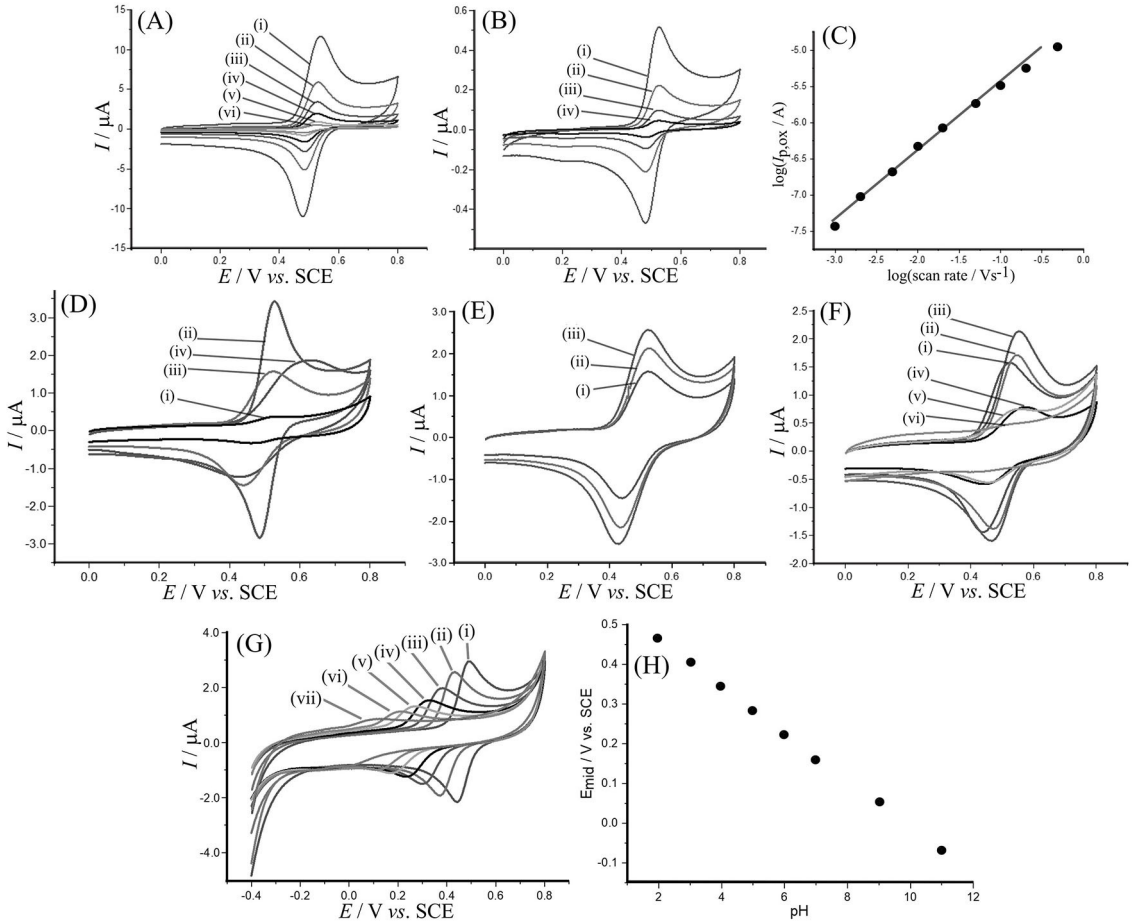

Figure 4. (A) Cyclic voltammograms (scan rates (i) 0.5, (ii) 0.2, (iii) 0.1, (iv) 0.05, (v) 0.02, (vi) 0.01 $V s^{-1}$) for a 3 mm diameter glassy carbon electrode with 2 µg PIM-EA-TB deposit (left 23 h in 0.1 M phosphate buffer pH 2 with 0.01 mM caffeic acid at 4 °C) immersed in 0.1 M phosphate buffer solution at pH 2. (B) As before, but with scan rates (i) 0.01, (ii) 0.005, (iii) 0.002, and (iv) 0.001 $V s^{-1}$. (C) Double logarithmic plot of anodic peak current *versus* scan rate; line indicating slope = 1.0. (D) Cyclic voltammograms (scan rate 0.1 $V s^{-1}$) for a 3 mm diameter glassy carbon electrode with 2 µg PIM-EA-TB deposit (left 23 h in 0.1 M phosphate buffer pH 2 with (i) 0.001, (ii) 0.01, (iii) 0.1 mM, and (iv) 1.0 mM caffeic acid at 4 °C) immersed in 0.1 M phosphate buffer solution at pH 2. (E) Cyclic voltammograms (scan rate 0.1 $V s^{-1}$) for a 3 mm diameter glassy carbon electrode with 2 µg PIM-EA-TB deposit (left (i) 17 h, (ii) 48 h, (iii) 119 h in 0.1 M phosphate buffer pH 2 with 0.1 mM caffeic acid at 4 °C) immersed in 0.1 M phosphate buffer solution at pH 2. (F) Cyclic voltammograms (scan rate 0.1 $V s^{-1}$) for a 3 mm diameter glassy carbon electrode with 2 µg PIM-EA-TB deposit (left 23 h in 0.1 M phosphate buffer (i) pH 2, (ii) pH 3, (iii) pH 4, (iv) pH 5, (v) pH 7, (vi) pH 9 with 0.1 mM caffeic acid at 4 °C) immersed in 0.1 M phosphate buffer solution at pH 2. (G) Cyclic voltammograms (scan rate 0.1 $V s^{-1}$) for a 3 mm diameter glassy carbon electrode with 2 µg PIM-EA-TB deposit (left 23 h in 0.1 M phosphate buffer pH 2 with 0.01 mM caffeic acid at 4 °C) in 0.1 M phosphate buffer solution consecutively at a pH of (i) 2, (ii) 3, (iii) 4, (iv) 5, (v) 6, (vi) 7, (vii) 9. (H) Plot of midpoint potential *versus* pH.

uptake is effective at pH values 2, 3, and 4 when the PIM-EA-TB is protonated. At pH 5 and pH 7 still significant redox peaks are observed, which suggests binding is not dependent on initial protonation of the PIM-EA-TB, but the guest-binding process may be progressing more slowly under neutral conditions. Finally, at pH 9 (Figure 4F(vi)) no more binding occurs. Formally, the caffeic acid binding process into PIM-EA-TB can be written as in equation 2 for pH <4 and written as in equation 3 for pH >4.

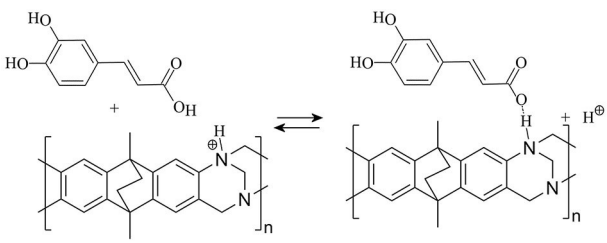

(2)

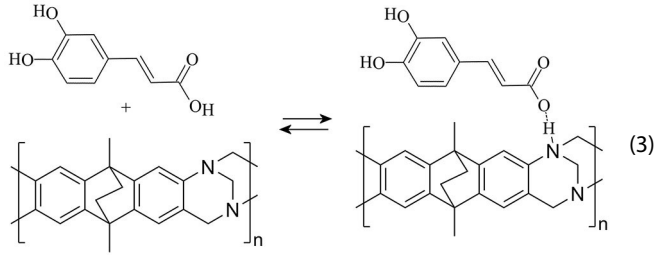

When changing the pH in the solution employed in cyclic voltammetry experiments, stable current data are obtained from pH 2 to pH 7 (see Figure 4G), but when going to more alkaline solution, the caffeic acid guest can be extracted from the PIM-EA-TB. The $pK_{A,1}$ for caffeic acid is 4.0 for the carboxylic acid proton (followed by $pK_{A,2}$ 8.5 and $pK_{A,3}$ 12.5 for the quinolic protons[26]), which is consistent with the effective extraction reaction happening at approximately pH >8.

2.2. Binding of Caffeic Acid into PIM-EA-TB Film Immobilised onto a Teflon Substrate with Microhole

PIM-EA-TB when applied to a Teflon substrate with 5 μm thickness and with a 10 μm diameter microhole, can be polarised to trigger ion transport (see Figure 1). The PIM-EA-TB film deposit is applied in a manner (on agarose gel) to leave the microhole mostly open as is shown in scanning electron microscopy (SEM) images in Figure 2. In energy-dispersive elemental mapping data, the F-elemental map is consistent with the Teflon and the C- and N-elemental maps clearly represent the PIM-EA-TB film (approx. 5 μm thick) on the opposite side seen through the microhole.

With aqueous 10 mM KCl (pH adjusted to pH 7) on both sides of the PIM-EA-TB film, a nearly symmetric exponentially increasing current response is observed (see Figure 5A(i)) consistent with a mixed conduction process with K^+ and Cl^- both contributing to the ionic current in the microporous PIM-

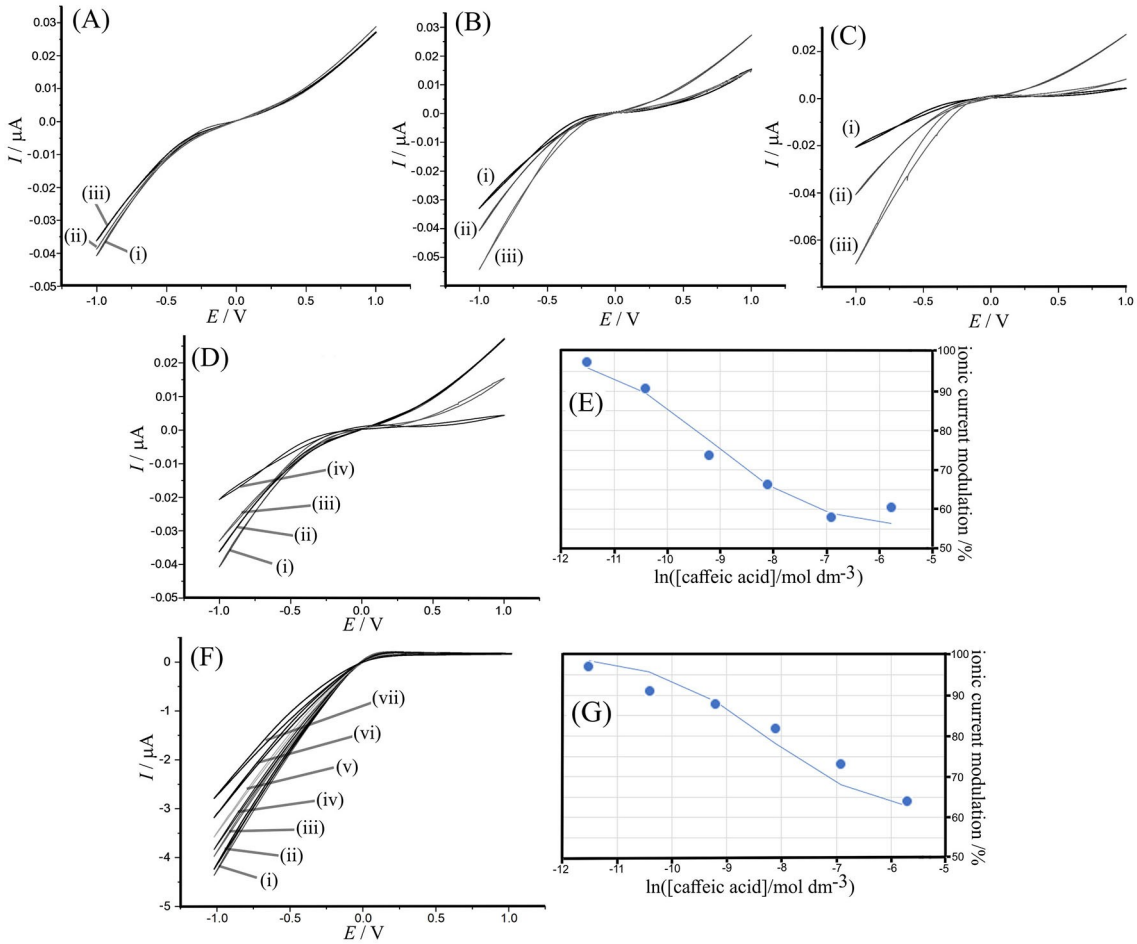

Figure 5. (A) Cyclic voltammetry data (scan rate 0.2 V s^{-1}) for a PIM-EA-TB film on 5 μm thick Teflon with a 10 μm diameter microhole with (i) aqueous 10 mM KCl (pH adjusted to 7) on both sides, (ii) 10 μM caffeic acid added to the working electrode compartment (pH 6.5), and (iii) HCl added to the working electrode compartment (to give pH 6.5). (B) As before, with (i) 100 μM caffeic acid added to the working electrode compartment (pH 4.8), (ii) aqueous 10 mM KCl (pH adjusted to 7) on both sides, and (iii) HCl added to the working electrode compartment (to give pH 4.8). (C) As before, with (i) 1000 μM caffeic acid added to the working electrode compartment (pH 4.0), (ii) aqueous 10 mM KCl (pH adjusted to 7) on both sides, and (iii) HCl added to the working electrode compartment (to give pH 4.0). (D) Comparison of voltammetry data for (i) 0. (ii) 10, (iii) 100, and (iv) 1000 μM caffeic acid in 10 mM KCl (working electrode compartment). (E) Plot of ionic current modulation versus logarithm of caffeic acid concentration without adjusting pH. (F) Comparison of voltammetry data for (i) 0, (ii) 10, (iii) 30, (iv) 100, (v) 300, (vi) 1000, and (vi) 3330 μM caffeic acid in 10 mM HCl at pH 2 (working electrode compartment). (G) Plot of ionic current modulation versus logarithm of caffeic acid concentration at pH 2.

EA-TB. Caffeic acid as a guest molecule is able to modify the behaviour. Figure 5A(ii) shows data for a low concentration of 0.01 mM caffeic acid being added into the solution compartment on the working electrode side. Only a very subtle change in ion current occurs. Figure 5B(ii) shows the effect of 0.1 mM caffeic acid, which is clearer. In the negative potential range, a slight decrease in current occurs and in the positive potential range a stronger decrease in ion current occurs. The resulting asymmetry is linked to ionic current rectification. However, the rectification effect is mainly due to pH rather than due to the caffeic acid binding *per se* as is shown in Figure 5B(iii). The solution pH change triggers the ionic diode effect due to gradual protonation of the tertiary amine in PIM-EA-TB. The presence of the caffeic acid causes the ionic currents to diminish.

Figure 5C shows data for 1 mM caffeic acid addition (to give pH 4.0). The same pattern is observed with pH triggering ionic diode effects, but the caffeic acid binding causing lower ion currents when compared to Figure 5C(iii) where HCl was added to give pH 4. Figure 5D shows the effect of caffeic acid more clearly. The anionic current at −1 V bias is lowered as the caffeic acid concentration increases. A plot in Figure 5E shows the percentage anionic current decrease as a function of caffeic acid concentration (without pH control). This data plot does resemble (at least approximately) a Langmuirian trend and an approximate fit of the data suggests a binding constant of 10^4 mol^{-1} dm^3 in reasonable agreement with data from film voltammetry experiments (see Figure 4). When repeating this experiment at pH 2 (10 mM HCl on both sides) a similar trend is observed with caffeic acid gradually blocking anion transport in the microchannels (Figure 5F). A plot of the ionic current modulation *versus* caffeic acid concentration (Figure 5G) shows less resemblance with Langmuirian characteristics but otherwise agrees with trends observed before. A higher concentration of caffeic acid does lower the transport of anionic species through the PIM-EA-TB film. It is of interest to explore the possible contributions or effects of caffeic acid on the chloride transport. In theory, caffeic acid could be blocking chloride transport sterically (causing a slower net diffusion) or caffeic acid could remove positive charges in the PIM-EA-TB (causing lower chloride concentration).

We speculate on the origin of the effect of reduced open diode current for increased binding of caffeic acid shown in Figures 5D, and 5F. The current reduction is either caused by a reduced mobility of anions in the PIM-EA-TB membrane, *i.e.*, by a reduced effective diffusivity due to geometrically blocked pores, or by the binding of caffeic acid leading to a deprotonation and lower net positive surface charge. Thus, a lower concentration of electrolyte anions is necessary to achieve charge neutrality, leading also to lower open currents. Figure 6 shows *qualitative* finite elements simulation of these possible effects.[18,27] Simulated voltammograms for reduced diffusivity in Figure 6A suggest that both currents for the open diode and for the closed diode are lowered. In contrast, voltammograms in Figure 6B for a reduced surface charge show that currents in the open diode state are lowered and currents in the closed diode state are increased (less net rectification due to a lower concentration of charge carriers in the polymer film). In the experimental data almost no effect on the closed diode state and a significant lowering of the current in the open diode state are observed. Therefore, a combination of both effects is shown in Figure 6C indicative of a compensation of effects of lower diffusivity and lower charge concentration in the closed diode state. A significant lowering of the current in the open diode state is simulated in qualitative agreement with experimental observations.

2.3. Transport of Caffeic Acid through a PIM-EA-TB Film Immobilised onto a Teflon Substrate with Microhole

To directly measure transport of caffeic acid (as a model for other hydrogen binding molecules) as a function of time, Q-TOF LC/MS analysis of the solution in the counter electrode compartment was performed. A 10×10 array of microholes is employed (see Figure 2) to enhance transport effects. Preliminary voltammetry data in Figure 6A(i) shows currents of approximately −30 μA for the array. In the presence of 1 mM caffeic acid the current is lowered to −8 μA (Figure 6A(ii)). This compares to the current for a single microhole under the same conditions −0.02 μA (Figure 5D(iv)). Some hysteresis in the current data suggests that a true steady state has in this case

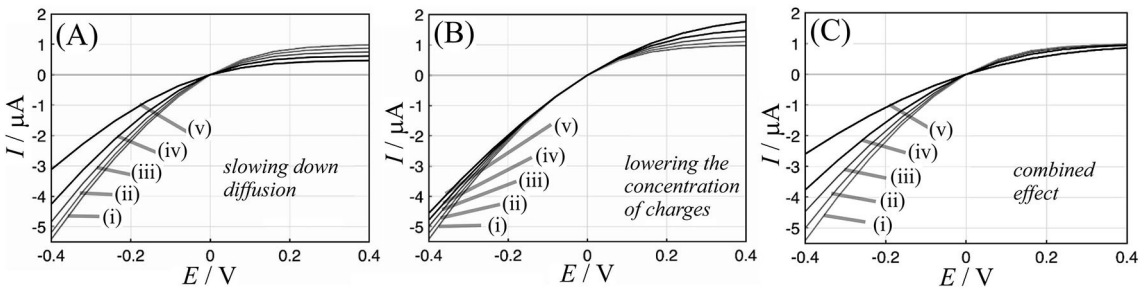

Figure 6. Qualitative finite element calculations for how diode behaviour is affected by binding of caffeic acid. (A) The diffusion coefficient for anions in the PIM-membrane is varied from (i) 100%, (ii) 80%, (iii) 60%, (iv) 40%, and (v) 20% to simulate the effect of caffeic acid blocking diffusion processes. (B) The concentration of fixed positive surface charges in the PIM-EA-TB membrane is varied from (i) 80 mM, (ii) 70 mM, (iii) 60 mM, (iv) 50 mM, to (v) 40 mM to simulate the effect of caffeic acid binding effectively removing charges. In (C) a combination of both effects is simulated with (i) to (v) indicating both slower diffusion and lower concentration of charge.

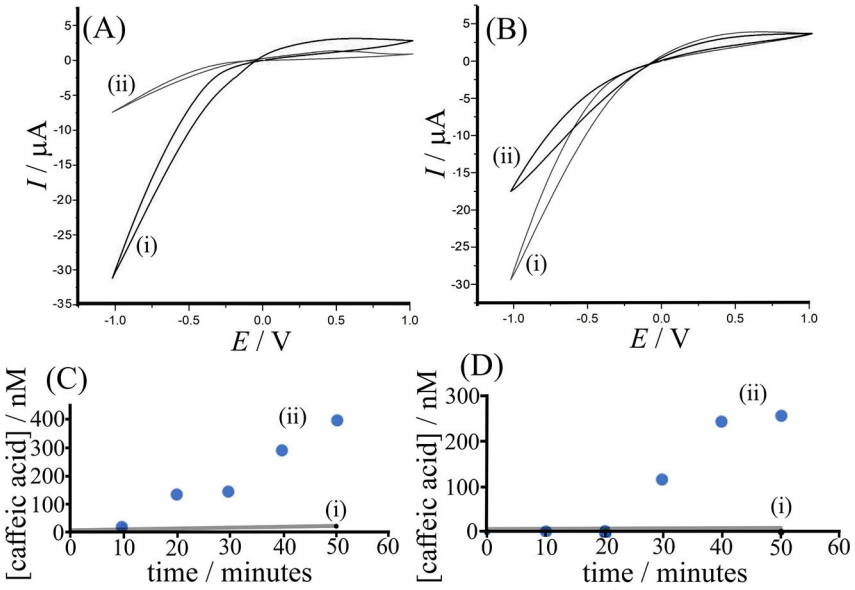

Figure 7. (A) Cyclic voltammetry data (scan rate 0.2 $V s^{-1}$) for a PIM-EA-TB film on 5 µm thick Teflon with an array of 10×10 microholes of 10 µm diameter with aqueous 10 mM KCl on both sides and with (i) 1 mM HCl or (ii) 1 mM caffeic acid added into the working electrode side. (B) Cyclic voltammetry data (i) before and (ii) after 50 minutes of ion transport at −1 V applied bias. (C) Plot of caffeic acid transportation (1 mM caffeic acid in 10 mM KCl in the working electrode compartment; pH 4; (i) without applied bias and (ii) with −1 V applied) as concentration in the counter electrode compartment *versus* time. (D) Plot of caffeic acid transportation in 10 mM HCl (1 mM caffeic acid in 10 mM HCl in the working electrode compartment; pH 2; (i) without applied bias and (ii) with −1 V applied).

not been reached and therefore the current observed at the array may appear slightly higher than expected based on simple scaling of the single microhole data.

When setting the applied bias in chronoamperometry mode to −1 V (open diode), it is possible to monitor both, the flow of charge and the concentration of caffeic acid with time. Figure 7C(i) shows that the cross-diffusion of caffeic acid without applied bias is minimal. However, with applied bias the caffeic acid is gradually increasing with time to approx. 0.4 µM after 50 minutes. The charge transport under these conditions (based on integrated current) was equivalent to a final solution concentration of 26 µM. Therefore only 1.5% of the observed charge transport is linked to the caffeic acid transport. This may be surprising given that a high concentration of caffeic acid is bound locally into the PIM-EA-TB under these conditions, but the observation can be rationalised based on an electroosmotic drag mechanism (*vide infra*). When repeating the transport investigation at pH 2 (10 mM HCl on both sides of the membrane and 1 mM caffeic acid add into the working electrode compartment), very similar observations are made. The cross-over of caffeic acid without applied bias remains negligible in the 50 minutes duration of the experiment. However, with −1 V applied bias, the transport of caffeic acid is clearly detected. Perhaps surprisingly, a very similar rate of caffeic acid transport is observed with about 0.25 µM detected concentration after 50 minutes. However, the current at pH 2 is higher and the integration of the current suggests in this case a final solution concentration of 170 µM. The observed value of 0.25 µM suggests a transfer efficiency of only 0.33%. In both cases there appears to be a delay in the first 10 to 20 minutes before significant caffeic acid transport is observed and this could be attributed to slow molecular transport of caffeic acid across the PIM-EA-TB film consistent with observations in voltammetry experiments.

What is intriguing in the data for caffeic acid transport at pH 4 (Figure 7C) and at pH 2 (Figure 7D) is the fact that almost identical amounts of caffeic acid were transferred. This could be a sign for a kinetically rate limited transport mechanism requiring the dissociation of the hydrogen bonding interaction and re-binding at the next available site. The binding constants were similar in acidic conditions (pH < 4) and in more neutral conditions (pH > 4) and therefore the activation barrier E_A for the transport could be similar. Figure 8 illustrates the suggested transport mechanism for caffeic acid in PIM-EA-TB based on dissociation/association "hops" from tertiary amine to tertiary

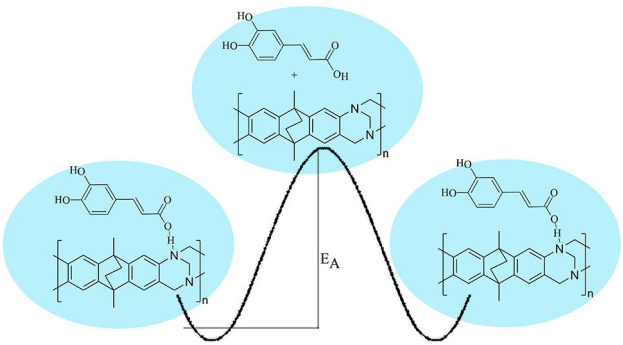

Figure 8. Schematic illustration of caffeic acid transport based on dissociation and re-association in the PIM-EA-TB microchannel.

amine (Figure 8). These hops are more effective with an underlying electroosmotic drag induced by the applied bias voltage and chloride anion transport. More experiments will be required to unravel the magnitude of the electroosmotic drag effect and the effects of applied bias voltage and other types of guest molecule.

3. Conclusion

It has been shown that caffeic acid accumulates into PIM-EA-TB from both acidic or neutral solution environments. Alkaline conditions can be employed to dissociate caffeic acid from the microporous polymer. As a film deposit on glassy carbon, PIM-EA-TB with caffeic acid immobilised shows cyclic voltammetry current responses very similar to those for caffeic acid in solution, although without diffusion characteristics, and at higher loadings peaks broaden due to "overcrowding". As a free-standing membrane, PIM-EA-TB shows modulation of ion currents due to caffeic acid binding. The caffeic acid binding effect appears to be closely related to observations in immobilised films and associated with hydrogen bonding effects. The transport of caffeic acid through PIM-EA-TB is electroosmotically driven. The mechanism is suggested to be kinetically limited due to the need for intermittent dissociation of the hydrogen bond. In the presence of electroosmotic drag induced by an applied bias voltage the caffeic acid is continuously transported (for both pH 2 or pH 4) and released into the opposite compartment. These measurements suggest that

(i) accumulation and transport of species across PIM-EA-TB films can be induced by hydrogen bonding interactions.
(ii) transport of guest species is linked to slow "hopping" diffusion and enhanced by an applied voltage causing electroosmotic drag effects within the PIM-EA-TB membrane.
(iii) the accumulation of guest molecules into PIM-EA-TB can modulate the ion transport in the micropores due to a combination of steric/blocking effects and charge removal effects.

In future, the properties of PIM materials could be tuned to allow selective binding and transport for example for guest molecules of medicinal interest or for applications in selective recovery of valuable molecules from waste streams. Further work will be required to unravel the mechanism of coupled transport of ionic and neutral species in rigid PIM microchannels and to quantify the magnitude of electroosmotic drag in these systems.

Acknowledgements

L.W. thanks the China Scholarship Council (201906870022) for a PhD stipend. K.M. acknowledges financial support from Provincie Gelderland.

Conflict of Interest

The authors declare no conflict of interest.

Keywords: ionic diode · hydrogen bonding · ion-channel · electroosmosis · uniporter

[1] S. N. Bush, T. T. Volta, C. R. Martin, *Nanomater.* **2020**, *10*, 571.
[2] W. Guo, Y. Tian, L. Jiang, *Acc. Chem. Res.* **2013**, *46*, 2834–2846.
[3] B. R. Putra, L. Tshwenya, M. A. Buckingham, J. Y. Chen, K. J. Aoki, K. Mathwig, O. A. Arotiba, A. K. Thompson, Z. K. Li, F. Marken, *Electroanalysis* **2021**, https://doi.org/10.1002/elan.202060614.
[4] D. P. He, E. Madrid, B. D. B. Aaronson, L. Fan, J. Doughty, K. Mathwig, A. M. Bond, N. B. McKeown, F. Marken, *ACS Appl. Mater. Interfaces* **2017**, *9*, 11272–11278.
[5] B. R. Putra, K. J. Aoki, J. Y. Chen, F. Marken, *Langmuir* **2019**, *35*, 2055–2065.
[6] B. D. B. Aaronson, D. Wigmore, M. A. Johns, J. L. Scott, I. Polikarpov, F. Marken, *Analyst* **2017**, *142*, 3707–3714.
[7] L. Tshwenya, F. Marken, O. A. Arotiba, *ChemElectroChem* **2019**, *6*, 3153–3145.
[8] B. R. Putra, K. Szot-Karpinska, P. Kudla, H. Yin, J. A. Boswell, A. M. Squires, M. A. Da Silva, K. J. Edler, P. J. Fletcher, S. C. Parker, F. Marken, *ACS Appl. Bio Mater.* **2020**, *3*, 512.
[9] E. Madrid, Y. Y. Rong, M. Carta, N. B. McKeown, R. Malpass-Evans, G. A. Attard, T. J. Clarke, S. H. Taylor, Y. T. Long, F. Marken, *Angew. Chem. Int. Ed.* **2014**, *53*, 10751–10754; *Angew. Chem.* **2014**, *126*, 10927–10930.
[10] N. B. McKeown, P. M. Budd, *Chem. Soc. Rev.* **2006**, *35*, 675–683.
[11] L. N. Wang, Y. Z. Zhao, B. B. Fan, M. Carta, R. Malpass-Evans, N. B. McKeown, F. Marken, *Electrochem. Commun.* **2020**, *118*, 106798.
[12] Z. X. Low, P. M. Budd, N. B. McKeown, D. A. Patterson, *Chem. Rev.* **2018**, *118*, 5871–5911.
[13] M. Carta, R. Malpass-Evans, M. Croad, Y. Rogan, J. C. Jansen, P. Bernardo, F. Bazzarelli, N. B. McKeown, *Science* **2013**, *339*, 303–307.
[14] R. Tan, A. Q. Wang, R. Malpass-Evans, R. Williams, E. W. Zhao, T. Liu, C. C. Ye, Z. Q. Zhou, B. P. Darwich, Z. Y. Fan, L. Turcani, E. Jackson, L. J. Chen, S. M. Y. Chong, T. Li, K. E. Jelfs, A. I. Cooper, N. P. Brandon, C. P. Grey, N. B. McKeown, Q. L. Song, *Nat. Mater.* **2020**, *19*, 195–199.
[15] Y. Y. Rong, D. P. He, A. Sanchez-Fernandez, C. Evans, K. J. Edler, R. Malpass-Evans, M. Carta, N. B. McKeown, T. J. Clarke, S. H. Taylor, A. J. Wain, J. M. Mitchels, F. Marken, *Langmuir* **2015**, *31*, 12300–12306.
[16] J. W. Jeon, J. Shin, J. Lee, J. H. Baik, R. Malpass-Evans, N. B. McKeown, T. H. Kim, J. C. Lee, S. K. Kim, B. G. Kim, *Appl. Surf. Sci.* **2020**, *530*, 147146.
[17] D. P. He, Y. Y. Rong, Z. K. Kou, S. C. Mu, T. Peng, R. Malpass-Evans, M. Carta, N. B. McKeown, F. Marken, *Electrochem. Commun.* **2015**, *59*, 72–76.
[18] K. Mathwig, B. D. B. Aaronson, F. Marken, *ChemElectroChem* **2018**, *5*, 897–901.
[19] L. N. Wang, R. Malpass-Evans, M. Carta, N. B. McKeown, F. Marken, *J. Solid State Electrochem.* **2020**, *24*, 2797–2806.
[20] R. Vinayagam, M. Jayachandran, B. J. Xu, *Phytother. Res.* **2016**, *30*, 184–199.
[21] C. F. Huang, S. S. Lin, P. H. Liao, S. C. Young, C. C. Yang, *Cellul. Mol. Immunol.* **2008**, *5*, 23–31.
[22] B. R. Putra, M. Carta, R. Malpass-Evans, N. B. McKeown, F. Marken, *Electrochim. Acta* **2017**, *258*, 807–813.
[23] D. P. Santos, M. F. Bergamini, A. G. Fogg, M. V. B. Zanoni, *Microchim. Acta* **2005**, *151*, 127–134.
[24] C. Giacomelli, K. Ckless, D. Galato, F. S. Miranda, A. Spinelli, *J. Braz. Chem. Soc.* **2002**, *13*, 332–338.
[25] X. Y. Xiong, X. F. Zhao, Z. H. Song, *Anal. Biochem.* **2014**, *460*, 54–60.
[26] R. Romero, P. R. Salgado, C. Soto, D. Contreras, V. Melin, *Front. Chem.* **2018**, *6*, 208.
[27] L. Tshwenya, F. Marken, K. Mathwig, O. A. Arotiba, *ACS Appl. Mater. Interfaces* **2020**, *12*, 3214–3224.

Manuscript received: March 31, 2021
Accepted manuscript online: May 7, 2021